

Nexus between directionality of terahertz waves and structural parameters in groove-patterned InAs

Jong-Hyuk Yim,¹ Kyunggu Min,¹ Hoonil Jeong,¹ Jin-Dong Song,² and Young-Dahl Jho^{1, a)}

¹⁾*School of Information and Communications, Gwangju Institute of Science and Technology, Gwangju 500-712, South Korea*

²⁾*Nano-Photonics Research Center, Korea Institute of Science and Technology, Seoul 136-791, South Korea*

(Dated: 28 August 2012)

We have performed terahertz (THz)-time domain spectroscopy in various geometries, for characterizing the directivity of THz waves emitted from groove-patterned InAs structures. First, we have identified two transient transport processes as underlying THz emission mechanisms in InAs epilayers with different thickness. The carrier drift around surface depletion region was predominant in thin sample group (10-70 nm) while the electronic diffusion was overriding the oppositely aligned drifting dipoles in thick sample group (370-900 nm) as revealed via amplitude change and phase reversal. By a combined use of electron-beam lithography and inductively coupled plasma etching in 1 μm -thick InAs epilayers, we have further periodically fabricated either asymmetric V-groove patterns or symmetric parabolic apertures. The THz amplitude was enhanced, particularly along *line-of-sight* transmissive direction when the groove patterns act as microscale reflective mirrors periodically separated by a scale of diffusion length.

I. INTRODUCTION

Over the past two decades, there has been great progress in the generating and utilizing terahertz (THz) waves for various applications, including imaging and communications.¹ Among various THz generation methods,² semiconductor surface emitters combined with pulsed laser excitations has been one of the well-established methods,^{3,4} which are described by either non-linear process⁵ or surge current model⁶; photo-carrier accelerations due to the surface field in wide band-gap semiconductors or dipole currents by the efficient separation between electrons and holes in narrow band-gap semiconductors (so-called, Photo-Dember effect).

Indium-based alloys are very attractive as contact-free THz emitters because of the large diffusion velocity difference between electrons and holes. Especially, InAs and InSb have the much higher electron mobilities (up to 30,000 $\text{cm}^2/\text{V}\cdot\text{s}$ and 76,000 $\text{cm}^2/\text{V}\cdot\text{s}$) than hole mobilities (up to 450 $\text{cm}^2/\text{V}\cdot\text{s}$ and 850 $\text{cm}^2/\text{V}\cdot\text{s}$).⁷ In the case of infrared pulse excitation ($\lambda \sim 800$ nm, the central wavelength of Ti:sapphire laser technology) on InAs and InSb, the absorption depth (~ 100 nm) is much shorter than the diffusion scale (~ 1 μm) and the large excess energy (> 1 eV) leads to the even higher mobilities of photo-excited carriers.⁸ In this context, InAs has been widely used as the most intense contactless THz emitter whereas InSb application has been limited probably due to the suppressed emission amplitude via the scattering of electrons into the L valley.⁶

Although THz efficiency of InAs is appropriate for contact-free THz applications, directivity of THz waves was hardly controllable. In general, semiconductor-based

THz time-domain spectroscopy (THz-TDS) under pulsed laser excitations are implemented based on many guiding components such as parabolic mirrors and lenses along reflective directions. Coordinating many optical components along the reflective directions leads to difficulty in controlling the direction of THz waves. Recently, THz studies based on diffusive semiconductors have been destined toward the easier availability and controllability of diffusions; THz microscopy system was instrumented with excellent spatial resolution using an optical fiber coupled with tilted InAs tips⁹ and THz amplitude enhancement was achieved by integrating periodic metal strip lines on $\text{In}_{0.53}\text{Ga}_{0.47}\text{As}$ layers for lateral diffusion currents.¹⁰ Furthermore, increased THz magnitude was reported in magnetic fields up to 8 T at 170 K,¹¹ or in microstructured large-area photoconducting emitter with external electric field up to 120 kV/cm at room temperature.¹² In this paper, we have implemented micro-scale groove patterns acting either as mirrors in IR range (in the case of V-groove patterns) or as grids for lateral symmetry breaking (in the case of parabolic apertures), aiming for characterizing the corresponding directivity of THz waves as being measured in reflective, transmissive and lateral detection geometries.

II. SAMPLES AND SCHEMES

The conventional THz-TDS measurements¹³ were performed under the illumination of a Ti:sapphire-based laser at 300K whose pulse duration was 150 fs pulse at the center wavelength of 800 nm. The samples were coordinated with photo-conductive antennas (PCA) in various detection geometries for characterizing THz waves along different directions as cartooned in Fig. 1. The IR laser source was incident on the sample surface at $\theta=45^\circ$ in the reflective geometry, otherwise at $\theta=90^\circ$ focused onto

^{a)} Electronic mail: jho@gist.ac.kr

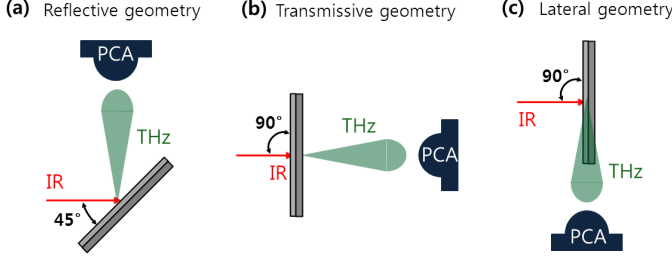


FIG. 1. Measurement schemes in (a) reflective (b) transmissive, and (c) lateral geometries.

a spot size of $800\ \mu\text{m}$. The pump beam supplies an excitation fluence of about $0.9\ \mu\text{J}/\text{cm}^2$ which corresponds to the linear regime in (100)-grown InAs.¹⁴ In the case of reflective and transmissive geometries, THz waves from samples are guided via a pair of off-axis parabolic mirrors into PCA whose sensitivity was optimized at around 1 THz. On the other hand, in the lateral detection geometry, PCA was placed very close to the sample (1 mm away from the sample edge) without guiding components.

The samples are classified into two categories; group **A**) bare InAs epilayers whose thickness was varied from 10 nm to 900 nm, and group **B**) 1 μm -thick samples with groove-patterns around 1 μm . The detailed structures and relevant fabrication procedures are described in section III-A for group **A** and in section III-B for group **B**, respectively.

III. RESULTS AND DISCUSSION

A. Determination of THz generation mechanism as a function of thickness

The transient carrier transport mechanisms contribute to the emission of THz waves when surfaces of semiconductor materials are illuminated by laser pulses; drift currents by photo-carriers around the surface depletion regions could be biased either towards or against the substrate side, depending on the doping type, whereas the diffusion (via photo-Dember effect) occurs inherently toward the substrate side. As discussed earlier, InAs is one of the most efficient contactless THz emitters, whose generation mechanism has been associated with photo-Dember effect in very thick samples ($> 100\ \mu\text{m}$)³. To examine the THz wave generation mechanisms in InAs layer whose thickness is comparable to or even smaller than the diffusion length scale, we have grown five unintentionally *n*-type doped InAs epilayers whose thickness was 10, 20, 70, 370, and 900 nm. To avoid the nonlinear effects, InAs was oriented along (100) direction, grown on GaAs substrate (thickness $\sim 300\ \mu\text{m}$) as shown in Fig. 2(a). To reduce the lattice mismatch and concomitant strain, $\text{AlAs}_{0.32}\text{Sb}_{0.68}$ layer (thickness $\sim 2.2\ \mu\text{m}$) was inserted between InAs and GaAs substrate. At 300 K,

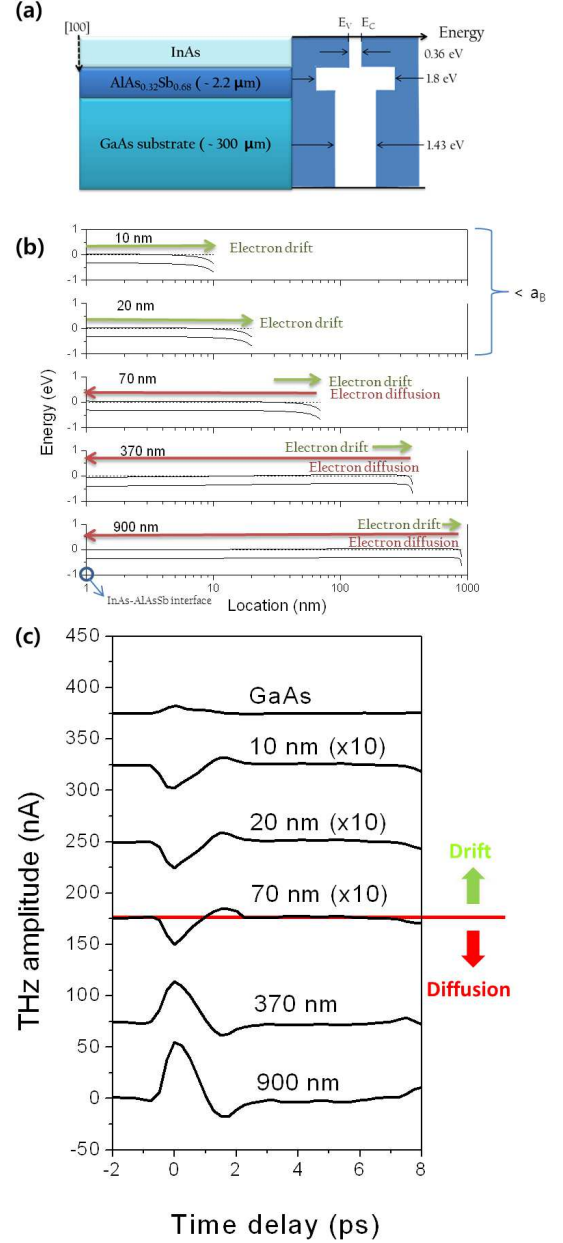


FIG. 2. (a) InAs epilayers grown on $\text{AlAs}_{0.32}\text{Sb}_{0.68}$ buffer layer and GaAs substrate, illustrated with the sketchy band gaps. (b) Energy band diagrams of InAs layers as a function of thickness. Green arrows and red arrows indicate electronic drift or diffusion field directions, respectively. (c) THz waveforms from InAs layers with different thicknesses, in comparison with GaAs substrate (from back side illumination of laser). Vertical arrows on the right-hand side divide THz emission regime, based either on the carrier drift motion (in thin sample group) or on the carrier diffusion (in thick sample group) with different phase.

bandgap of materials are roughly illustrated, in parallel with sample structures on the right-hand side of Fig. 2(a). It is known that the optical rectification effect is

minimized along (100) direction¹⁵, thus, the transport mechanisms are discussed from a perspective viewpoint of THz wave generation in this and following subsections.

In the energy band diagram of Fig. 2(b) as a function of sample thickness and n -type sheet carrier densities (measured elsewhere)¹⁶, we found that the electronic drift due to the tilted potentials at the surface was set to be opposite to the direction of carrier diffusion if available. In the quantum-confined scale of 10 and 20 nm (thin sample group) which is smaller than the exciton Bohr radius of 36 nm in a bulk InAs¹⁷, the diffusive features are mostly suppressed in contrast to the transient electron-hole separation due to the tilted potential shape around the surface. In 70 nm-thick layer (thin sample group), the direction of transient drift currents are opposite to that of the partly allowed diffusion currents cancelling the net current flow. In thick sample group of 370 nm and 900 nm, the carrier diffusion (mostly dominated by electrons) can occur throughout the InAs layer, whereas the oppositely aligned drifting electrons are spatially localized within the surface depletion layer of about 50 nm.

Such thickness-dependent transport features are further confirmed by tracing the amplitudes and phases of THz waves which are associated with the transient gradient of dipole density, ambient electric field strength and dipole polarizations. Fig. 2(c) shows the THz-TDS results in reflection geometry as a function of InAs layer thickness. As a reference, GaAs substrate was illuminated from backward direction and the corresponding THz waves were displayed on top of Fig. 2(c). The THz amplitude showed rapid increment after 70 nm. This amplitude variation in samples thicker than the absorption depth (~ 100 nm) and exciton Bohr diameter is understood based on the efficient carrier diffusion and subsequent THz wave radiation. We further note that the opposite direction of electronic motions between the thin samples (dominated by the carrier drift) and thick sample group (dominated by the diffusion) led to the opposite phase of THz waves as indicated by the vertical arrows in Fig. 2(c). Intriguingly, 70 nm-thick sample showed even smaller THz amplitude than thinner samples, which testifies to the barely initiated diffusions cancelling out the influence from electron drift along opposite direction. In this regard, in a thickness range larger than the 370 nm, the underlying THz wave generation mechanisms is based on the electronic diffusion which will be further engineered for directional control of THz waves in the following section **III-B**.

B. Directional THz emission modulated by groove-patterns

InAs epitaxial layers (thickness $\sim 1 \mu\text{m}$) were grown by molecular beam epitaxy along (100) direction on a GaAs substrate (thickness $\sim 500 \mu\text{m}$) as shown in figure 3(a). InAs layers were p -type doped with a concentra-

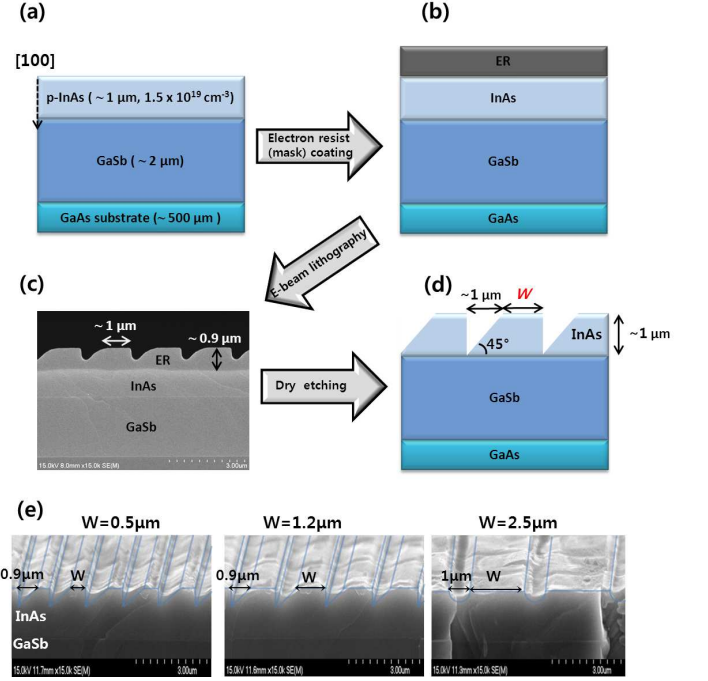


FIG. 3. Schematic fabrication processes for forming the groove patterns: (a) the bare InAs epilayer structure, (b) electron-resist (ER) layer, coated on InAs structure, (c) SEM image after E-beam writing and developing, and (d) finalized structure by dry etching process. (e) SEM images of the fabricated structures with different values of W ($0.5 \mu\text{m}$ and $1.2 \mu\text{m}$ with trapezoidal patterns, and $2.5 \mu\text{m}$ with parabolic patterns).

tion of $\sim 1.5 \times 10^{19} \text{ cm}^{-3}$. A GaSb layer (thickness $\sim 2 \mu\text{m}$) was inserted as a buffer layer to reduce the interfacial lattice mismatch. To fabricate the groove patterns, electron resist (ER) was coated on top of InAs layer (Fig. 3(b)). The electron beam writing was adapted for developing groove patterns on the ER using shot-modulation in electron-beam lithography, followed by dry etching process using inductively coupled plasma etcher with combined use of composite gas of Cl_2 and N_2 for forming groove patterns. Fig. 3(d) shows the proposed structure with a trapezoidal groove angle of 45° with pattern width (W). The pattern width W was varied from $0.5 \mu\text{m}$ and $1.2 \mu\text{m}$ to $2.5 \mu\text{m}$ as shown in the SEM images of Fig. 3(e). It is notable that W was varied in a comparable scale to the electronic diffusion length in InAs ($\sim 1.3 \mu\text{m}$).¹⁸ The blue lines in Fig. 3(e) are guide to eyes for intended structures either with trapezoid-shaped grooves (in the case of $W=0.5$ and $1.2 \mu\text{m}$) or with parabolic-aperture grooves (in the case of $W=2.5 \mu\text{m}$). During the fabrications, the edges of groove patterns were slightly deformed, identified as the deviation of SEM images from the blue lines in Fig. 3(e). The area of groove-patterned region was estimated to be about $5 \times 1 \text{ mm}^2$.

Figure 4(a) shows a comparison between THz emission in reflective and in transmissive geometries in InAs bare

samples as a reference. As expected, the signal along the transmissive direction in Fig. 4(a) was mostly suppressed since the diffusive dipoles are mostly aligned along the growth direction with relatively much weaker lateral components and the subsequent THz radiation patterns are perpendicular to transient currents. In addition, the THz waves generated within the InAs layer along the lateral direction are restrictedly coupled with the internal radiation cone along surface-normal direction due to the large mismatch in refractive index at the surface (the refractive index of ~ 3.5 for InAs compared to ~ 1.0 for free space).¹⁹ The small and slow oscillatory features after 10 ps could be ascribed to Fabry-Perot interference between air-InAs and air-GaAs interfaces.

In the case of groove-patterned structures, in clear contrast to the bare layer, we found that the THz signals were significantly enhanced along transmissive direction as shown in Fig. 4(b). The incident beam was normal to the surface and polarized linearly and orthogonally to the striped patterns. Due to the formation of diffusion-induced transient dipoles along the surface via the reflected IR pulses toward the lateral direction, the THz radiation patterns are now profiled toward the line-of-sight direction, manifested by the increased amplitude in Fig. 4(b). Particularly, a sample with W of $1.2\ \mu\text{m}$ turned out to be the most efficient which was in a similar scale to the diffusion length in InAs.¹⁸ The signals from a sample with W of $0.5\ \mu\text{m}$ was less enhanced in that the electrons can easily diffuse from one side to the other, thus, could be attracted to the rather stationary holes. In the case when $W = 2.5\ \mu\text{m}$, the patterns could break the lateral symmetry of diffusion but with limited lateral diffusion efficiency, considering the large laser spot size compared to W . Some further arguments could be raised regarding the results in Fig. 4(b); 1) the Fabry-Perot interference was persistent in patterned structures, implying that the refractive index contrast at the interfaces was still persistent. Thus, the radiation outcoupling efficiency between the inside the materials and the free space seems not influenced by the groove patterns. 2) photocarriers generated in slope pyramid plane in the trapezoidal patterns could undergo the diffusion along the (110) direction with the much reduced carrier mobility and with heavier effective mass compared to those along (100) direction, which leads to the reduced photo-Dember field and the limited amplitude enhancement. 3) The not-perfectly defined faces of groove patterns could lead to the scattering loss of the incident IR photons. The pattern scale was much smaller than the THz wavelength, possibly triggering the Rayleigh scattering. Such arguments could be further discussed elsewhere based on spectrum-domain studies and angle-dependent amplitude analysis. Along the lateral direction (Fig. 4(c)), in clear contrast to transmissive direction, we could not observe the signal changes between patterned structures and the bare samples. The signals in general in Fig. 4(c) were much weaker than those in other geometries, possibly due to the slightly misaligned THz guiding optics,

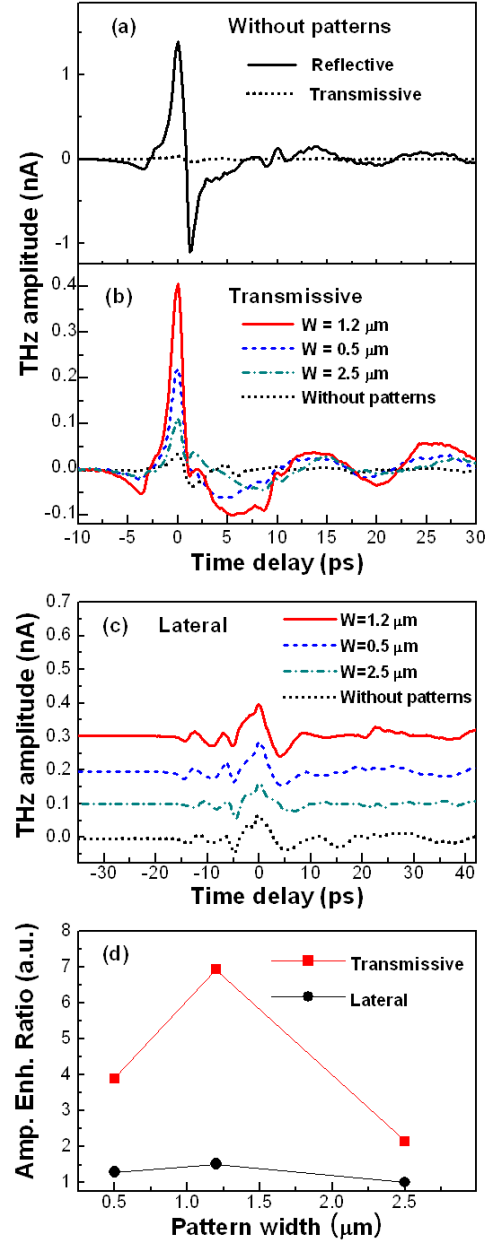


FIG. 4. Time-domain THz-TDS signals measured from (a) bare InAs layers in the reflective or transmissive geometries, (b) groove-patterned structures in comparison with the bare InAs layer (black-dotted line) in the transmissive geometry, and (c) groove-patterned structures in comparison with the bare InAs layer in the lateral geometry. (d) Amplitude enhancement ratio of THz waves along transmissive and lateral directions, normalized by amplitudes in bare InAs layer.

the scattering losses at the rough facets, and attenuation inside the medium. As a comparative purpose, we normalized THz signal amplitudes from the patterned structures either in the transmissive or in lateral geometries by those from the bare InAs layer in Fig. 4(d). THz wave amplitudes were increased significantly depending

on the structural parameters of the periodic groove patterns, only along the line-of-sight transmission direction. The highest amplitude enhancement ratio at $W=1.2\ \mu\text{m}$ indicates that the optimized adjustment of W could be further obtained around the diffusion length.

IV. SUMMARY

For a purpose of directional control of THz waves, $1\ \mu\text{m}$ -thick InAs epilayers were processed to have either 45 degree reflectors (with gap width W of 0.5 or $1.2\ \mu\text{m}$) or parabolic apertures with W of $2.5\ \mu\text{m}$. The W and the sample thickness were designed to be similar to the diffusion length in which scale the THz emissions are predominantly generated by photo-Dember effect. We have performed THz-TDS measurements excited with a pulsed IR source of Ti:sapphire laser at 300 K. THz-TDS resulted in a dramatic contrast among different emission directions. In patterned structures, specifically with mirror-like trapezoidal patterns, THz signals were enhanced along the transmissive direction whereas the lateral THz emission was not varied by the additional patterning. The enhancement was rather associated with the efficient lateral dipole formation, optimized when W was similar to the diffusion length.

ACKNOWLEDGMENTS

This work was supported by the Bio-Imaging Research Center at GIST and by the Basic Science Research Program through the National Research Foundation of Korea (NRF-2009-0090559). The work at KIST was supported by the KIST Institutional Program and

the Korea-Sweden Research Cooperation Program.

- ¹M. Tonouchi, Nat. Photonics **1**, 97 (2007).
- ²K. Sakai, *Terahertz Optoelectronics* (Springer, Berlin, 2005).
- ³X.-C. Zhang, J. T. Darrow, B. B. Hu, D. H. Auston, M. T. Schmidt, P. Tham, and E. S. Yang, Appl. Phys. Lett. **56**, 2228 (1990).
- ⁴R. Ascazubi, I. Wilke, K. Denniston, H. Lu, and W. J. Schaff, Appl. Phys. Lett. **84**, 4810 (2004).
- ⁵S. L. Chuang, S. Schmitt-Rink, B. I. Greene, P. N. Saeta, and A. F. J. Levi, Phys. Rev. Lett. **68**, 102 (1992).
- ⁶P. Gu, M. Tani, S. Kono, K. Sakai, and X.-C. Zhang, J. Appl. Phys. **91**, 5533 (2002).
- ⁷A. Nainani, D. Kim, T. Krishnamohan, K. Saraswat, "Hole Mobility and its Enhancement with Strain for Technologically Relevant III-V Semiconductors," Proceedings of SISPAD 2009, pp. 47-50.
- ⁸T. Dekorsy, H. Auer, H. J. Bakker, H. G. Roskos, and H. Kurz, Phys. Rev. B **53**, 4005 (1996).
- ⁹M. Yi, K. Lee, J. Lim, Y. Hong, Y. D. Jho, and J. Ahn, Opt. Express **18**, 13693 (2010).
- ¹⁰G. Klatt, B. Surrer, D. Stephan, O. Schubert, M. Fischer, J. Faist, A. Leitenstorfer, R. Huber, and T. Dekorsy, Appl. Phys. Lett. **98**, 021114 (2004).
- ¹¹R. McLaughlin, A. Corchia, M.B. Johnston, Q. Chen, C.M. Ciesla, D.D. Arnone, G.A.C. Jones, E.H. Linfield, A.G. Davies, and M. Pepper, Appl. Phys. Lett. **76**, 2038 (2000).
- ¹²A. Dreyhaupt, S. Winnerl, T. Dekorsy, and M. Helm, Appl. Phys. Lett. **86**, 121114 (2005).
- ¹³D. Grischkowsky, S. Keiding, M. van Exter, and C. Fattinger, J. Opt. Soc. Am. B, **7**, 2006 (1990).
- ¹⁴M. Reid and R. Fedosejevs, Appl. Phys. Lett. **86**, 011906 (2005).
- ¹⁵K. Liu, J. Xu, T. Yuan and X.-C. Zhang, Phys. Rev. B **73**, 155330 (2006).
- ¹⁶H. Jeong, S.H. Shin, S.Y. Kim, J.D. Song, S.B. Choi, D.S. Lee, J. Lee, and Y.D. Jho, Curr. Appl. Phys. **12**, 668-672 (2012).
- ¹⁷H. Fu, L.-W. Wang, and A. Zunger, Phys. Rev. B **59**, 5568 (1999).
- ¹⁸C. T. Que, T. Edamura, M. Nakajima, M. Tani, and M. Hangyo, **48**, 010211 (2009).
- ¹⁹M.B. Johnston, D.M. Whittaker, A. Corchia, A.G. Davies, and E.H. Linfield, Phys. Rev. B, **65**, 165301 (2002).